Taylor & Francis
Taylor & Francis Group

FOCUS ISSUE REVIEW

OPEN ACCESS   Check for updates

Carbonate apatite artificial bone

Kunio Ishikawa and Koichiro Hayashi

Department of Biomaterials, Faculty of Dental Science, Kyushu University, Higashi-ku, Japan

ABSTRACT

Bone apatite is not hydroxyapatite (HAp), it is carbonate apatite (CO_3Ap), which contains 6–9 mass% carbonate in an apatitic structure. The CO_3Ap block cannot be fabricated by sintering because of its thermal decomposition at the sintering temperature. Chemically pure (100%) CO_3Ap artificial bone was recently fabricated through a dissolution–precipitation reaction in an aqueous solution using a precursor, such as a calcium carbonate block. In this paper, methods of fabricating CO_3Ap artificial bone are reviewed along with their clinical and animal results. CO_3Ap artificial bone is resorbed by osteoclasts and upregulates the differentiation of osteoblasts. As a result, CO_3Ap demonstrates much higher osteoconductivity than HAp and is replaced by new bone via bone remodeling. Granular-type CO_3Ap artificial bone was approved for clinical use in Japan in 2017. Honeycomb-type CO_3Ap artificial bone is fabricated using an extruder and a $CaCO_3$ honeycomb block as a precursor. Honeycomb CO_3Ap artificial bone allows vertical bone augmentation. A CO_3Ap-coated titanium plate has also been fabricated using a $CaCO_3$-coated titanium plate as a precursor. The adhesive strength is as high as 76.8 MPa, with excellent tissue response and high osteoconductivity.

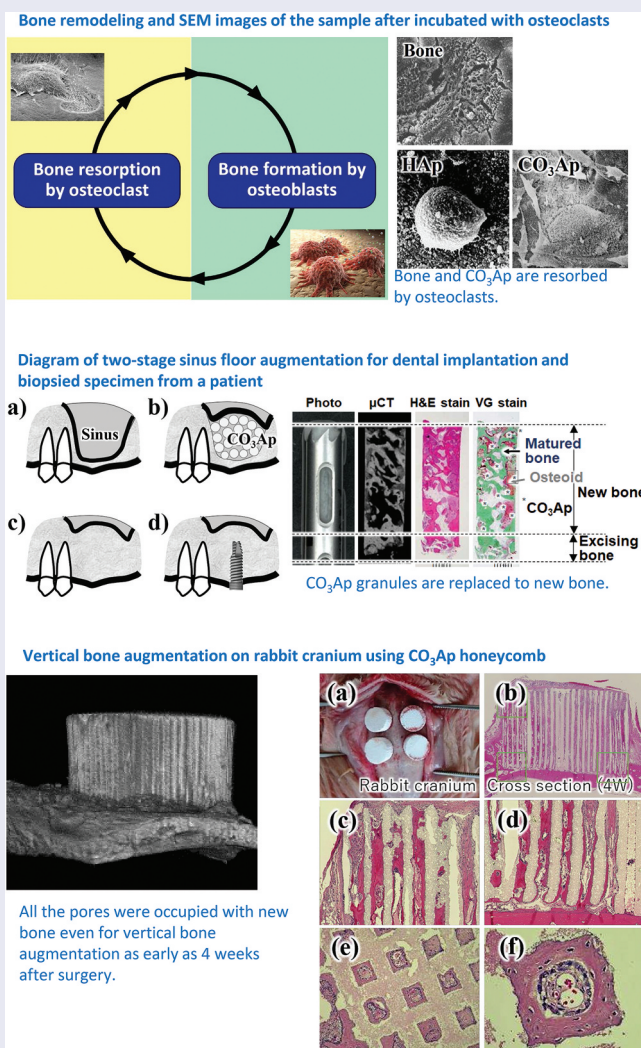Bone remodeling and SEM images of the sample after incubated with osteoclasts

Bone resorption by osteoclast

Bone formation by osteoblasts

Bone

HAp CO_3Ap

Bone and CO_3Ap are resorbed by osteoclasts.

Diagram of two-stage sinus floor augmentation for dental implantation and biopsied specimen from a patient

a) b) Sinus CO_3Ap

c) d)

Photo   µCT   H&E stain   VG stain

Matured bone
Osteoid
CO_3Ap New bone
Excising bone

CO_3Ap granules are replaced to new bone.

Vertical bone augmentation on rabbit cranium using CO_3Ap honeycomb

All the pores were occupied with new bone even for vertical bone augmentation as early as 4 weeks after surgery.

(a) Rabbit cranium   (b) Cross section (4W)

(c) (d)

(e) (f)

CONTACT Kunio Ishikawa ✉ ishikawa@dent.kyushu-u.ac.jp Department of Biomaterials, Faculty of Dental Science, Kyushu University, 3-1-1 Maidashi, Higashi-ku, Fukuoka 812-8582, Japan

Article classifications: 211 Scaffold/Tissue engineering/Drug delivery<200 Applications

1. Bone apatite

Animals with a skeleton are classified as invertebrates or vertebrates. The skeleton of invertebrates is composed of calcium carbonate ($CaCO_3$) and is likely derived from elements found in seawater. In contrast, vertebrates, including humans, have a skeleton of carbonate apatite [CO_3Ap: $Ca_{10-a}(PO_4)_{6-b}(CO_3)_c$] instead of $CaCO_3$ [1–5].

A key difference between $CaCO_3$ and CO_3Ap skeletons is phosphorous. Phosphorous or phosphate is important in energy metabolism in the process of generating energy or adenosine triphosphate (ATP). Invertebrates can use phosphates present in seawater, even though their concentrations are low (1.3 µmol/L). However, vertebrates living on the land need to store phosphorous in the body. During evolution from invertebrates to vertebrates, bone became the storage organ of phosphorous in vertebrates. In other words, CO_3Ap was chosen as bone apatite as a result of evolution from invertebrates to vertebrates.

CO_3Ap or bone apatite should be amenable for use as artificial bone. However, sintered hydroxyapatite (HAp) instead of CO_3Ap has been used as a typical artificial bone since the 1970s. This is because the thermal decomposition of CO_3Ap begins at approximately 400°C, which prevents the fabrication of sintered CO_3Ap. Recently, 100% chemically pure CO_3Ap blocks were fabricated through a dissolution–precipitation reaction in an aqueous solution using a $CaCO_3$ block as a precursor.

2. CO_3Ap fabrication though dissolution–precipitation reaction using a precursor

There are three key requirements for compositional transformation through the dissolution–precipitation reaction. First, the solubility of the precursor should be higher than that of the final product. Second, any component that is lacking must be supplied from the aqueous solution. Third, precipitates or crystals of the final product should have the ability to interlock with one another to maintain the shape of the block.

CO_3Ap is a thermodynamically stable phase under physiological conditions. It is not soluble under physiological conditions. Moreover, CO_3Ap crystals can interlock. Many compounds are more soluble than CO_3Ap, and thus can be precursors for the fabrication of CO_3Ap through dissolution–precipitation reactions including $CaCO_3$ [6–18], α-tricalcium phosphate [19–24], dicalcium phosphate dihydrate [25,26], and $CaSO_4$ [27–30]. Moreover, a component that is lacking can be supplied from aqueous solution.

One of the ideal precursors is $CaCO_3$. It has low solubility in aqueous solution at neutral pH and contains both calcium and carbonate. Chemically pure $CaCO_3$ blocks can be easily fabricated by simply exposing calcium hydroxide [$Ca(OH)_2$] compact to carbon dioxide (CO_2) [eq. (1)].

$$Ca(OH)_2 + CO_2 \rightarrow CaCO_3 + H_2O \qquad (1)$$

The compositional transformation of CO_3Ap from $CaCO_3$ requires phosphate. The $CaCO_3$ block needs to be immersed in a phosphate salt solution for this compositional transformation.

When $CaCO_3$ is immersed in an aqueous solution, it dissolves and supplies Ca^{2+} and CO_3^{2-} [eq. (2)]. If other ions are absent, the water becomes saturated with $CaCO_3$. However, the situation is different when water contains PO_4^{3-}. In that case, the phosphate salt aqueous solution can be supersaturated with respect to CO_3Ap when both Ca^{2+} and CO_3^{2-} are supplied by the dissolution of $CaCO_3$. Thus, Ca^{2+}, PO_4^{3-}, and CO_3^{2-} precipitate as CO_3Ap [eq (3)], and the precipitated CO_3Ap crystals interlock with one another. Continuous dissolution–precipitation reactions lead to the compositional transformation from $CaCO_3$ to CO_3Ap, maintaining the macroscopic structure of the precursor.

$$CaCO_3 \rightarrow Ca^{2+} + CO_3^{2-} \qquad (2)$$

$$Ca^{2+} + PO_4^{3-} + CO_3^{2-} \rightarrow Ca_{10-a}(PO_4)_{6-b}(CO_3)_c \qquad (3)$$
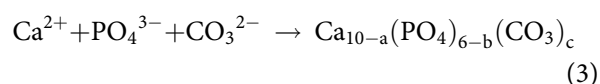
Other useful precursors are $CaSO_4 \cdot 2H_2O$, α-tricalcium phosphate [α-TCP: $Ca_3(PO_4)_2$], and dicalcium phosphate dihydrate [DCPD: $CaHPO_4 \cdot 2H_2O$]. However, sulfate ions tend to remain in the apatitic structure when $CaSO_4 \cdot 2H_2O$ is used as a precursor. CO_3Ap containing a small amount of HAp tends to form when α-TCP or DCPD are used as precursors because of the competitive reaction to form CO_3Ap and HAp. Therefore, $CaCO_3$ appears to be an ideal precursor. Fabrication of CO_3Ap based on compositional transformation through a dissolution–precipitation reaction using $CaCO_3$ as a precursor may have arisen during the evolution of vertebrates from invertebrates.

3. CO_3Ap and bone remodeling

3.1. Bone remodeling process

Bone remodeling involves the replacement of old bone and autograft by new bone. Osteoclasts resorb the old bone or autograft, followed by the formation of new bone by osteoblasts (Figure 1). Apatite is osteoconductive. Therefore, osteoblasts are active on their surfaces, although the degree of activity can differ depending on the type of apatite. The activity of osteoclasts also differs according to the type of apatite. Figure 2 displays representative scanning electron microscopy (SEM) images of osteoclasts incubated on the surfaces of bone, HAp, and CO_3Ap. The absence of osteoclastic resorption with HAp [6] is evidence that HAp cannot be replaced with new bone because osteoclast resorption does not occur. In
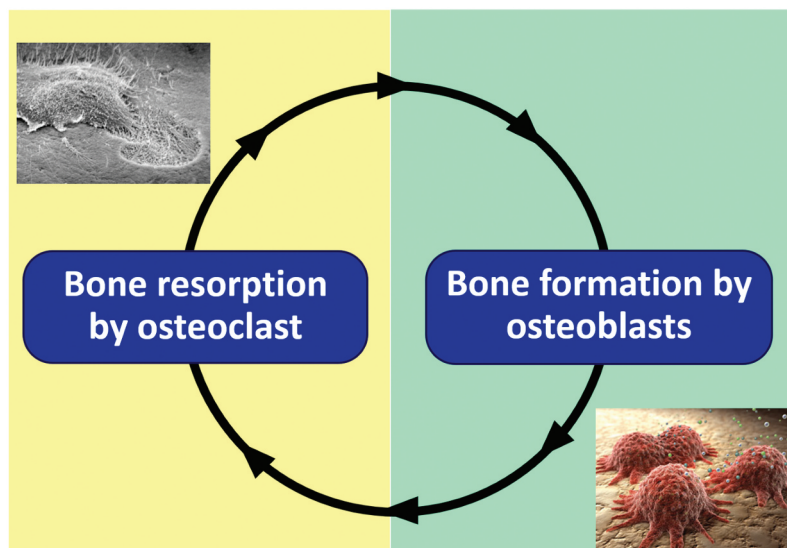
Figure 1. Graphical image of bone remodeling performed by osteoclasts and osteoblasts.
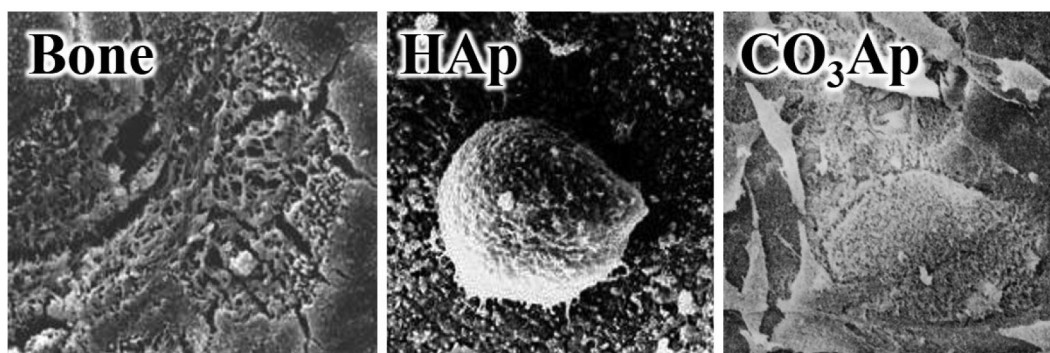

Figure 2. SEM images of bone, sintered HAp, and CO_3Ap when osteoclasts were incubated on their surfaces [6].

contrast, osteoclastic resorption occurs for bone and CO_3Ap.

Osteoclasts form Howship's lacunae and decrease the pH inside the lacunae to pH 3–5, leading to the dissolution of bone apatite. Thus, osteoclasts resorb apatite by dissolving it using a weak acid (Figure 3).

Figure 4 summarizes the solubilities of HAp and CO_3Ap as a function of pH. At physiological pH or pH 7.4, CO_3Ap is thermodynamically the most stable phase. This may explain why bone apatite is CO_3Ap. However, under weakly acidic conditions produced by osteoclasts or at a pH of 3–5, the solubility of CO_3Ap is higher than that of HAp. Therefore, CO_3Ap dissolves in weakly acidic conditions and is resorbed by osteoclasts, whereas HAp does not appreciably dissolve under weakly acidic conditions and is not resorbed by osteoclasts.

3.2. Differentiation of osteoblasts

Osteoblastic activity is the counterpart of osteoclastic activity in bone remodeling (Figure 3). One of the parameters of osteoblastic activity is differentiation.

Osteoblastic differentiation markers include type I collagen, alkaline phosphatase, osteopontin, and osteocalcin (Figure 5) [31]. Human bone marrow cells (hBMCs) incubated on CO_3Ap demonstrated much higher expression than HAp. Upregulation of osteoblast differentiation is likely one of the causes of the higher osteoconductivity of CO_3Ap artificial bone, in addition to the activation of osteoblasts through cell-cell interactions with osteoclasts.

3.3. Histological findings

Figure 6 summarizes the representative results of Villanueva Goldner (VG) histologic staining comparison of CO_3Ap and sintered HAp (Neobone®) used for reconstruction of mandibular bone defects adjacent to dental implants in beagle dogs 4 weeks after reconstruction surgery [32]. In VG staining, mature bone is stained green. Reconstruction of a defect with HAp involves the formation of only a limited amount of bone at the defect site, on the surface of the bone defect, and adjacent to the dental implant. This is one reason why no artificial bones have been approved
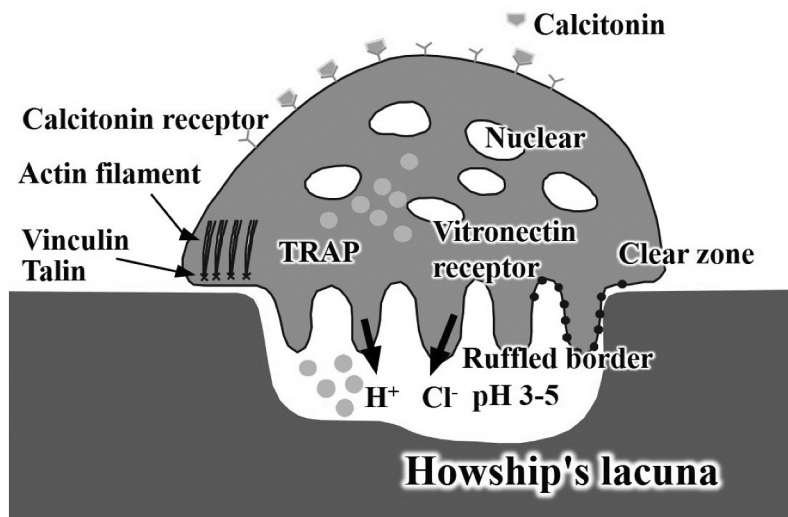
Figure 3. Graphical image of osteoclasts.

for implant-related bone defect reconstruction surgeries in Japan. In contrast, more bone forms even at the center of bone defects reconstructed using CO_3Ap. The surfaces of bone defects and dental implants become covered with bone. The documented bonding that results between bone, CO_3Ap, and dental implant clearly indicating the usefulness of CO_3Ap as an artificial bone for dental implants.

3.4. Clinical trials

The first human clinical trial was performed at three university hospitals in patients requiring sinus floor augmentation [33,34]. Figure 7 illustrates the procedure for two-stage sinus floor augmentation [34]. After the sinus floor membrane was elevated with a mucosal elevator, CO_3Ap granules were placed in the elevated space (Figure 7(b)). Implant placement was planned for 8 ± 2 months after the augmentation. Prior to implantation, a bone biopsy can be performed using a trephine bur (Figure 7(c)).

Figure 8 summarizes the micro-computed tomography (μ-CT) images and the appearance of biopsy tissue stained with hematoxylin and eosin (H-E) or VG. CO_3Ap granules were replaced with new bone, even though a small amount of CO_3Ap granules remain at this stage [34]. The presence of both mature bone and osteoids indicated active bone remodeling. Few inflammatory cells or foreign-body giant cells were observed in the biopsy specimens. The mean preoperative residual bone height of 3.4 ± 1.3 mm was increased to 13.0 ± 1.9 mm by the sinus floor augmentation using the CO_3Ap granules. Since the height after sinus floor augmentation is sufficient for dental implants, all patients received dental implants without any problems [33,34]. Based on the trial results, CO_3Ap granules were approved for clinical use as Cytrans Granules (GC Co, Tokyo, Japan) by
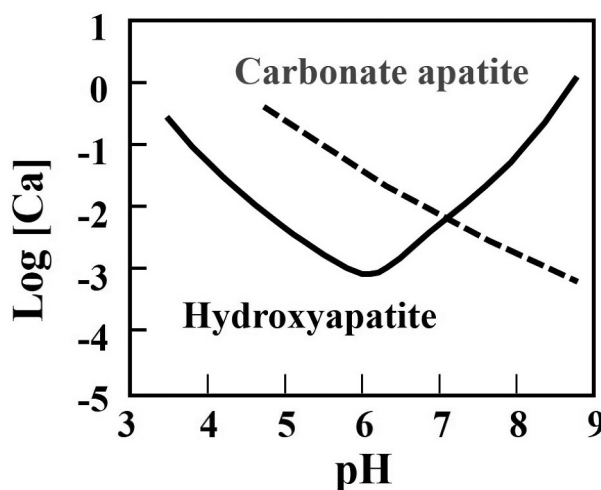

Figure 4. Solubility of carbonate apatite and hydroxyapatite in body fluid in terms of calcium concentration as a function of pH [14].

the Pharmaceuticals and Medical Devices Agency (PMDA) in 2017. The chemically pure CO_3Ap granules are the first to be commercially available globally and the first artificial bone that can be used for bone reconstruction aimed at dental implantation in Japan.

4. CO_3Ap honeycomb artificial bone

Not only composition but also architecture play important roles in governing the ability of artificial bone. In other words, regulation of architecture may be one of the important keys for artificial bone to demonstrate the similar osteoconductivity of autograft. One of the attractive architectures is the honeycomb. Fabrication of the CO_3Ap honeycomb by the dissolution–precipitation reaction requires a precursor. In general, a honeycomb is fabricated by extruding a raw material through a honeycomb die
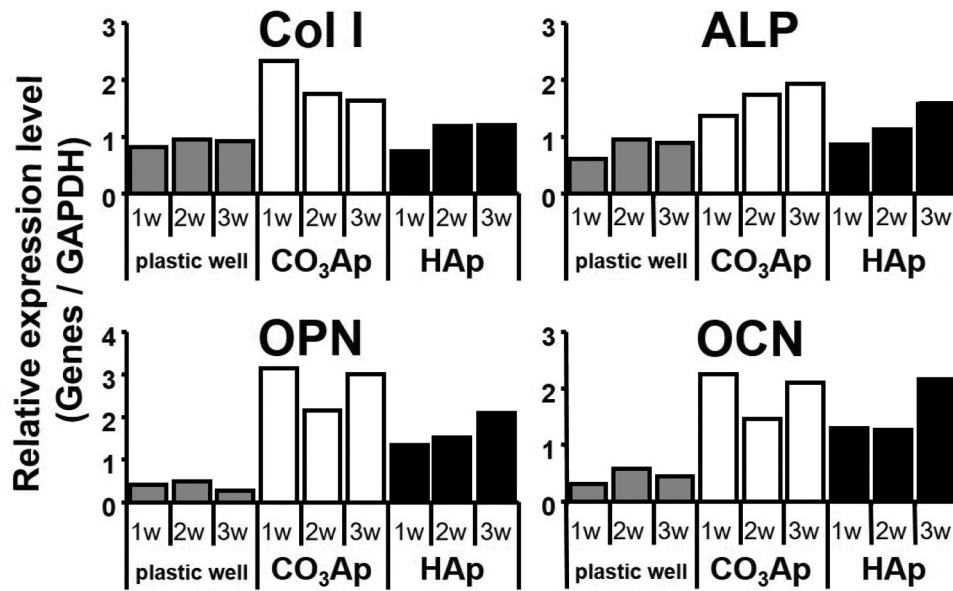
Figure 5. Relative gene expression levels of type I collagen, alkaline phosphatase, osteopontin, and osteocalcin on the surface of plastic well, CO_3Ap, and sintered HAp [31].
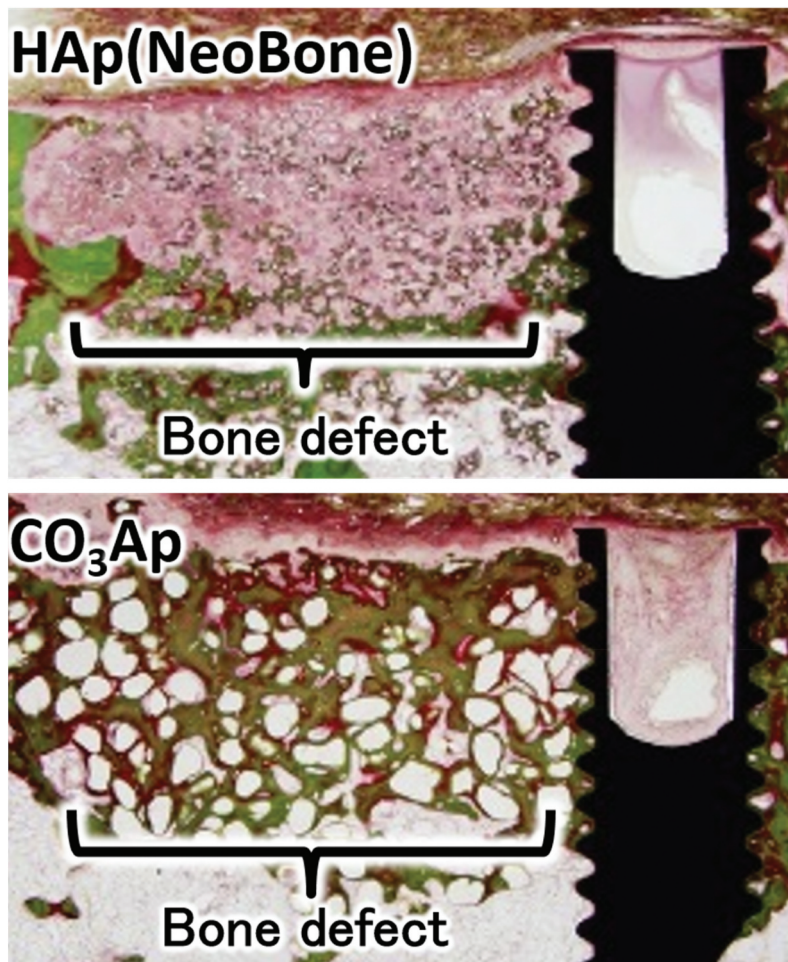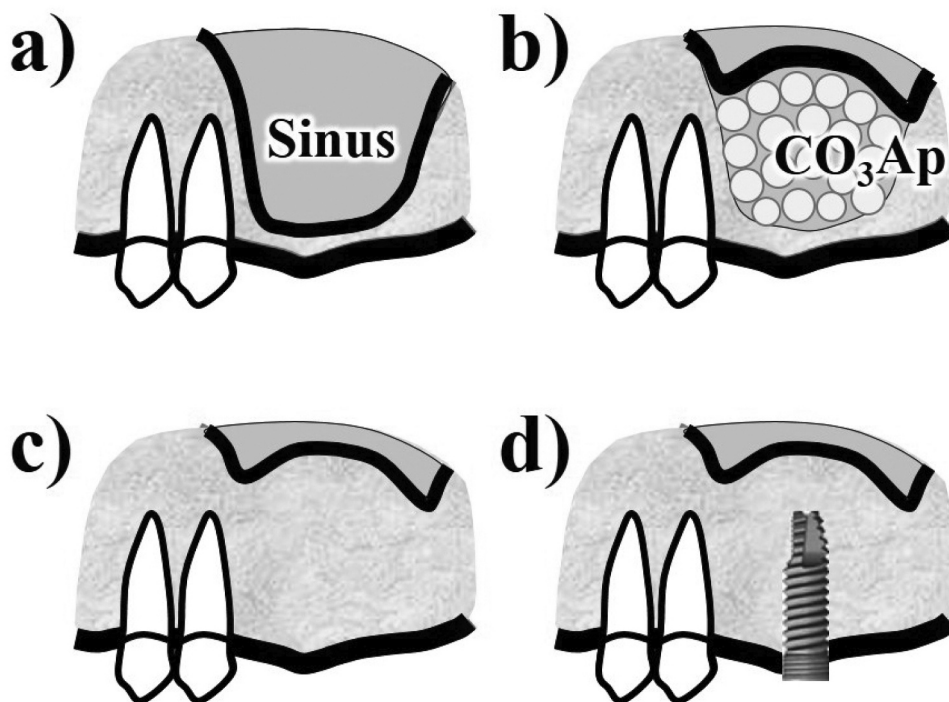

Figure 6. VG-stained histological image of sintered HAp (Neobone®) and CO_3Ap 4 weeks after reconstruction surgery of beagle dogs' mandibular bone defect adjacent to a dental implant [32].

Figure 7. Diagram of two-stage sinus floor augmentation for dental implantation. (a) before operation, (b) filling CO_3Ap granule after elevation of sinus floor membrane, (c) before biopsy which was performed 8 ± 2 months after the surgery, (d) after dental implantation.
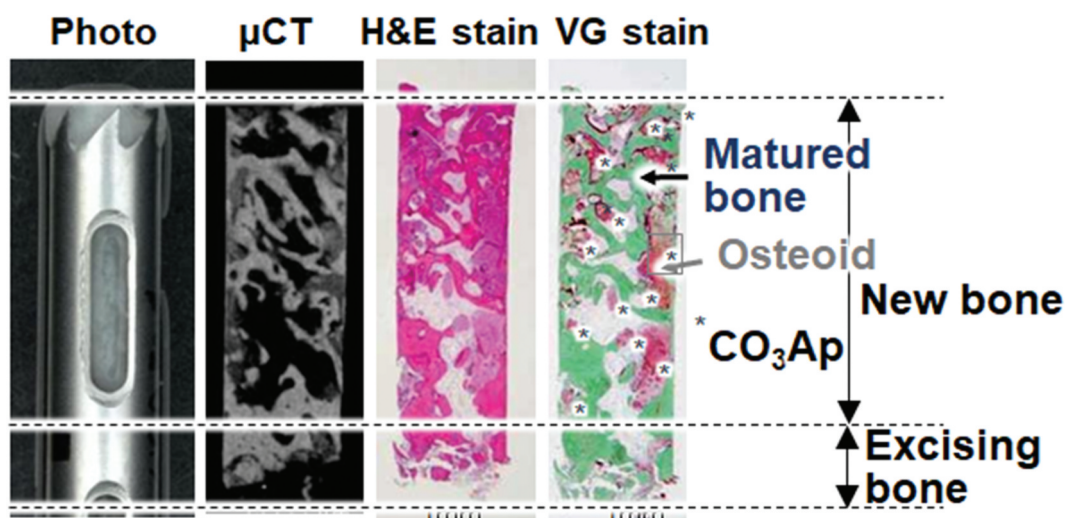
Figure 8. Photo, μ-CT scanning, H-E and VG staining of a histological specimen biopsied from a patient who underwent two-stage sinus floor augmentation for dental implantation [34].

(Figure 9). An organic binder is necessary for extrusion. Therefore, the organic binder must be eliminated in the subsequent debindering.

The $CaCO_3$ honeycomb becomes a CO_3Ap honeycomb by immersion in a phosphate salt aqueous solution based on compositional transformation through a dissolution–precipitation reaction that maintains the honeycomb structure. Figure 9 shows typical SEM images of $CaCO_3$ and CO_3Ap honeycombs. The macroscopic honeycomb structure was maintained during the compositional transformation. However, the microstructure is changed during the dissolution–precipitation

reaction, indicating a dependence on the crystal structure of each honeycomb composition.

Figure 10 displays a representative histological image one month after reconstruction of the femoral bone defect using the CO_3Ap honeycomb [13]. Tissue penetration into all pores of CO_3Ap honeycomb is evident. At higher magnification, the new bone formation at the pore surface of CO_3Ap honeycomb is evident. The presence of osteoclasts and osteoblasts on the surface of the newly formed bone indicates active bone remodeling. Osteocytes are also observed within the bone matrix. Interestingly, numerous vascular
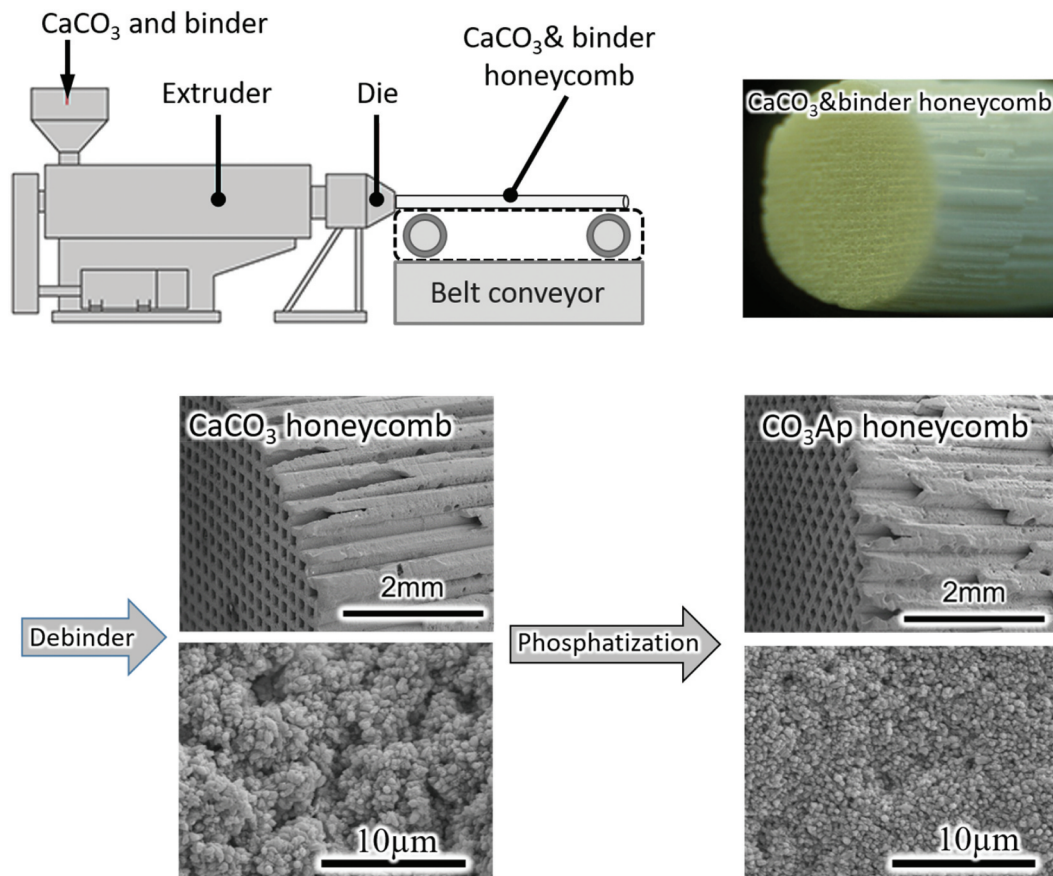
Figure 9. Diagram of honeycomb fabrication process and SEM images of $CaCO_3$ and CO_3Ap honeycombs.
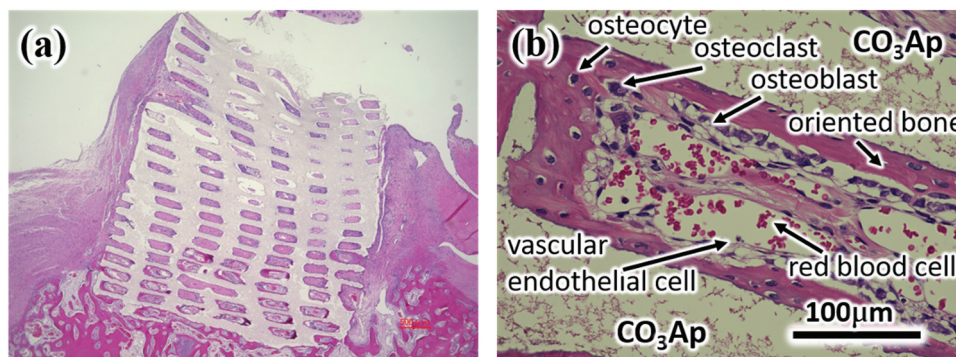

Figure 10. H-E stained histological image 4 weeks after rabbit femoral bone defect was reconstructed using a CO_3Ap honeycomb [13]. The (b) is a locally magnified photograph of (a).

endothelial cells and red blood cells are found inside the pores, indicating the formation of blood vessels [12].

Vertical bone augmentation can be performed using the CO_3Ap honeycomb. Figure 11 summarizes the results of vertical bone augmentation on rabbit cranium. New bone formation was confirmed 4 weeks after implantation, even at the top of the CO_3Ap honeycomb (Figure 11(b)). Magnified images of the top (Figure 11(c)) and bottom (Figure 11(d)) parts of the CO_3Ap honeycomb along the pores, cross section of the CO_3Ap honeycomb at mid-height (Figure 11(e)), and new bone formation at the pore surface of the CO_3Ap honeycomb (Figure 11(f)) are

shown. The same histological results were obtained for vertical bone augmentation as for femoral bone defect augmentation. Osteoclasts, osteoblasts, and osteocytes were also observed. In addition, numerous vascular endothelial cells and red blood cells were found inside the pores.

A comparison of the cell and tissue responses among the CO_3Ap, HAp, and β-TCP honeycombs has also been reported [35]. Alkaline phosphatase (ALP) activity is an index of osteoblast maturation. ALP activity of MC3T3-E1 cells 7 days following seeding was approximately two-fold higher for the CO_3Ap honeycomb than for β-TCP and HAp honeycombs (Figure 12).
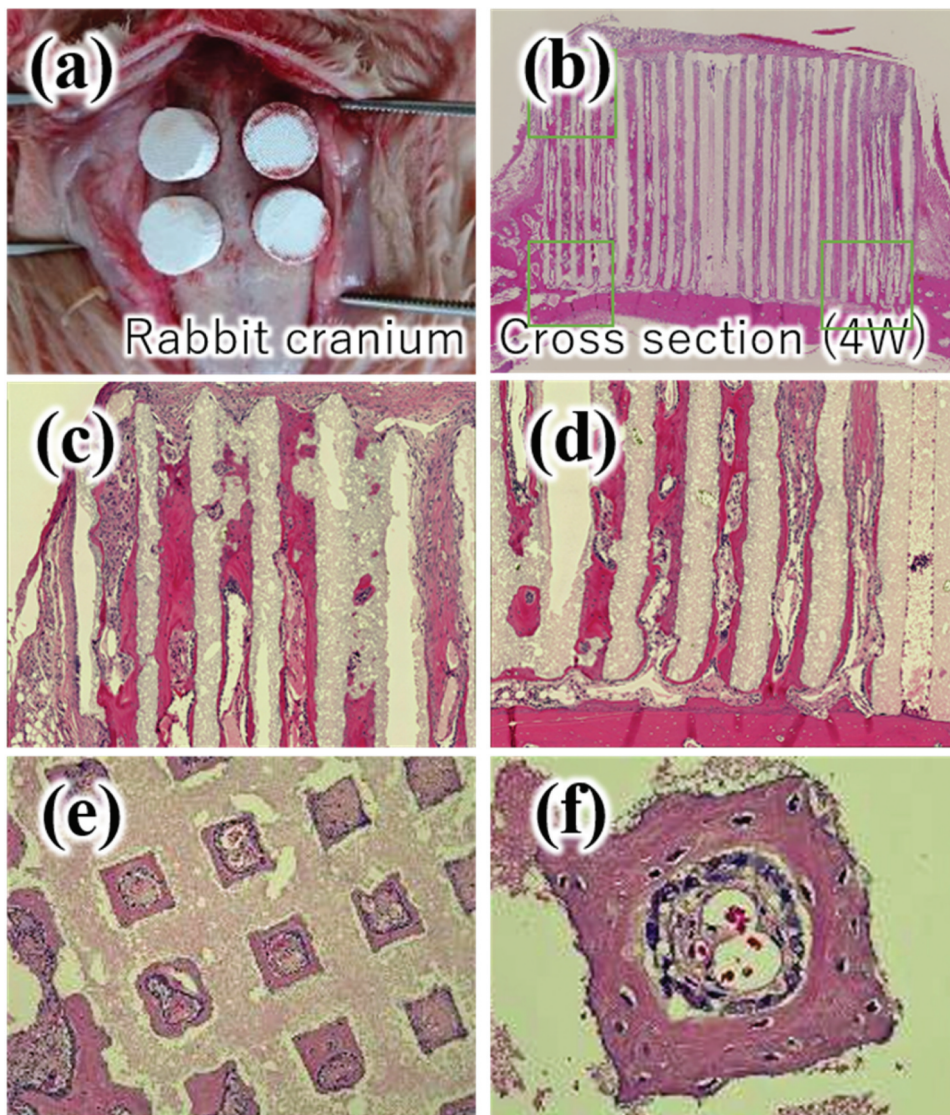
Figure 11. Implantation procedure (a) and H-E stained histological images, (b)-(f), 4 weeks after vertical bone augmentation on rabbit cranium [13]. (c) top of the CO_3Ap honeycomb, (d) bottom parts of the CO_3Ap honeycomb, (e) CO_3Ap honeycomb at mid-height, (f) higher magnification of (e).
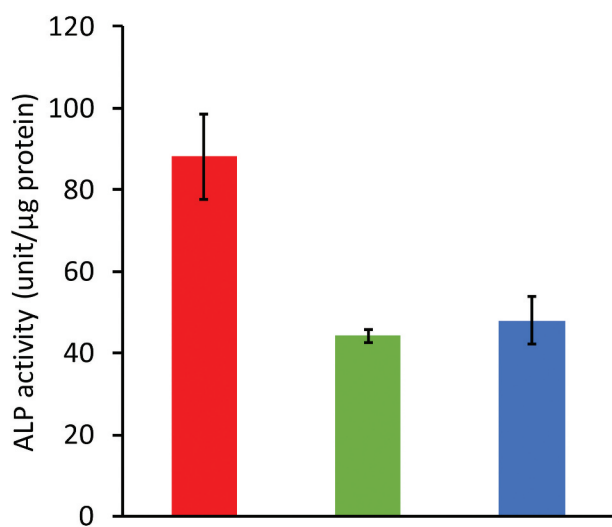
Figure 12. Effects of honeycomb's composition on MC3T3-E1 cell differentiation *in vitro*. ALP activity of cells cultured for 7 days on CO_3Ap, HAp, and β-TCP honeycombs [35].

Figure 13 summarizes μ-CT and H-E stain histological findings 4 weeks after bone defects made at the distal epiphysis of rabbit femurs were reconstructed with CO_3Ap, HAp, and β-TCP honeycombs [35]. In the case of the CO_3Ap honeycomb, new mature bone formed along the walls surrounding the macropores. Osteoblasts were detected along the new bone, osteoclasts were detected on the material surface, and blood vessels were detected in the macropores (Figure 13(c), Figure 13(g)). In the HAp honeycomb, immature bone, but not mature bone, was observed in only a small portion of the macropores at 4 weeks post-operation (Figure 13(e),Figure 13(h)). Osteoblasts, osteoclasts, and blood vessels were not observed in any macropores in the HAp honeycomb, whereas these cells and tissues were present in every macropore examined in the CO_3Ap honeycomb. Even at 12 weeks after surgery, almost all macropores were occupied by immature bone, and osteoblasts and osteoclasts were
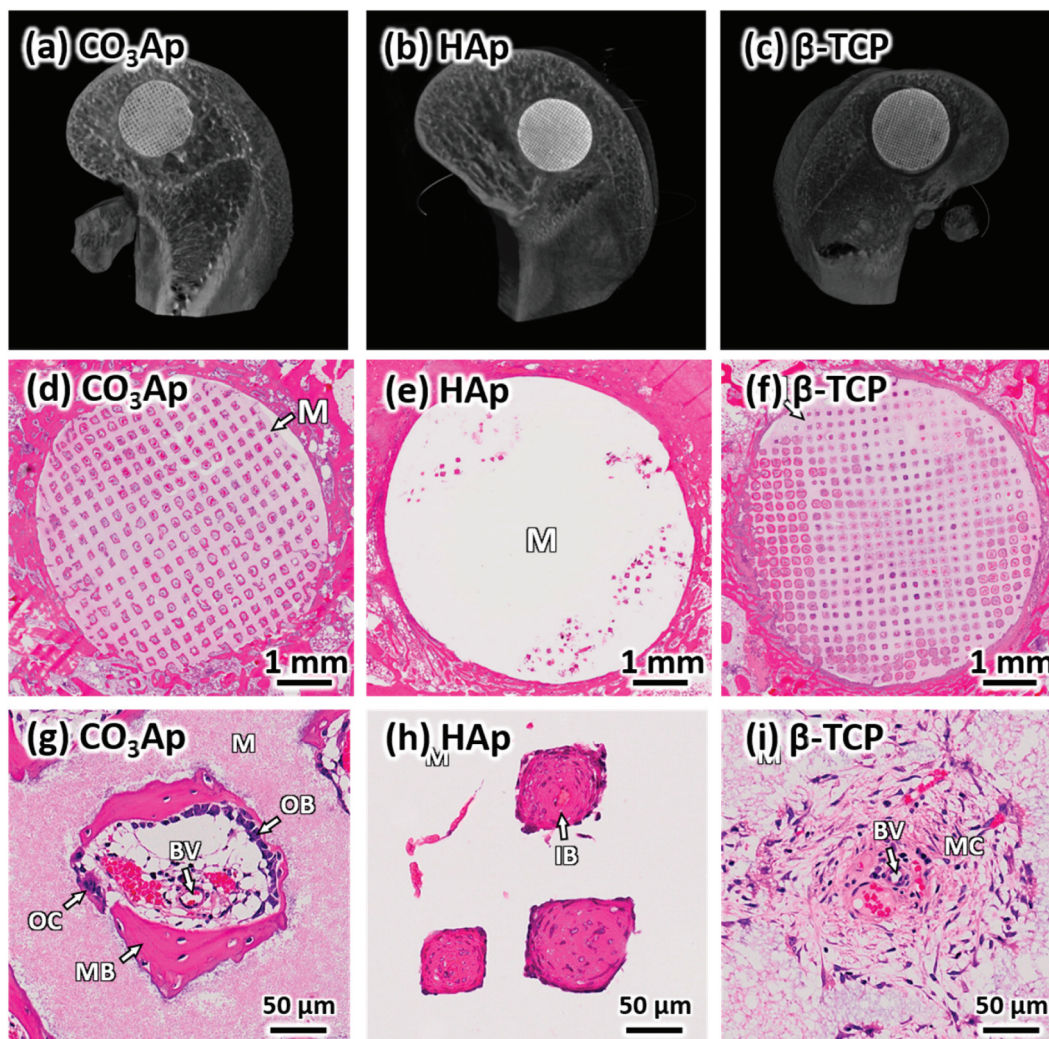
Figure 13. μ-CT images, (a–c), and HE-stained histological images, (d-i), of bone defects 4 weeks after reconstruction with CO_3Ap (a, d, g), HAp (b, e, h), and β-TCP (c, f, i) honeycombs. 'OB,' 'OC,' 'MB,' 'IB,' 'MC,' 'M,' 'BV,' and 'AC' indicate osteoblast, osteoclast, new mature bone, immature bone, mesenchyme, material, blood vessel, and adipose cell, respectively [35].

not observed in the macropores. In the case of β-TCP honeycomb 4 weeks after surgery, almost all macropores were filled with mesenchyme, and no osteoblasts or osteoclasts were observed in the macropores (Figure 13(f,Figure 13(i)). New mature bone formation was observed within a small portion of macropores. The area of mature bone at 4 and 12 weeks after surgery is summarized in Figure 14 along with the remaining mineral area. The area of mature bone area was significantly larger for CO_3Ap honeycomb compared to that of HAp and β-TCP honeycombs. Remaining materials area was largest for HAp honeycomb followed by CO_3Ap honeycomb and β-TCP honeycomb for both 4 and 12 weeks after surgery.

5. CO_3Ap coated titanium plate

Titanium (Ti) is used as an implant device because of its high mechanical strength and ease of osseointegration [36,37]. In particular, surface-roughed Ti implants demonstrate greater osseointegration and a higher implantation success rate. However, osteogenesis of Ti,

even with a roughened surface, is poorer than that of osteoconductive materials like apatite. Therefore, initial loosening of Ti implants is a problem for early loading [38, 39, 40].

Ti roughened surface coated with CO_3Ap may be an ideal Ti implant because of its pronounced osteoconductivity and replacement by new bone. CO_3Ap coated Ti (CO_3Ap–Ti) can be fabricated by compositional transformation through a dissolution–precipitation reaction using calcite-coated titanium ($CaCO_3$–Ti) as a precursor [39–41].

In this process, $CaCO_3$–Ti is established on the roughened surface Ti by wetting the Ti with an ethanol solution of $Ca(NO_3)_2$, followed by heating at 550°C in a CO_2 gas atmosphere. This results in the thermal decomposition of $Ca(NO_3)_2$ and its carbonation. CO_3Ap–Ti is then fabricated through a dissolution–precipitation reaction in an aqueous solution of Na_2HPO_4 using $CaCO_3$–Ti as a precursor.

The adhesion strengths of $CaCO_3$–Ti and CO_3Ap–Ti are as high as 56.6 and 76.8 MPa, respectively. Figure 15 summarizes the VG-stained histological results 4 weeks
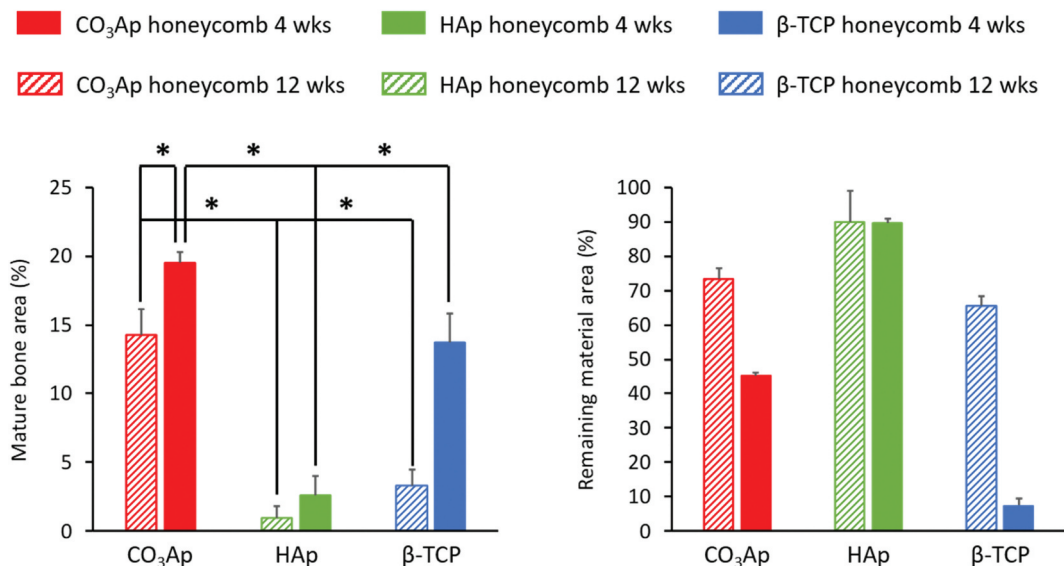
Figure 14. Mature bone area and remaining material area of bone defects 4 and 12 weeks after reconstruction with CO_3Ap, HAp, and β-TCP honeycombs. *p < 0.05 [35].
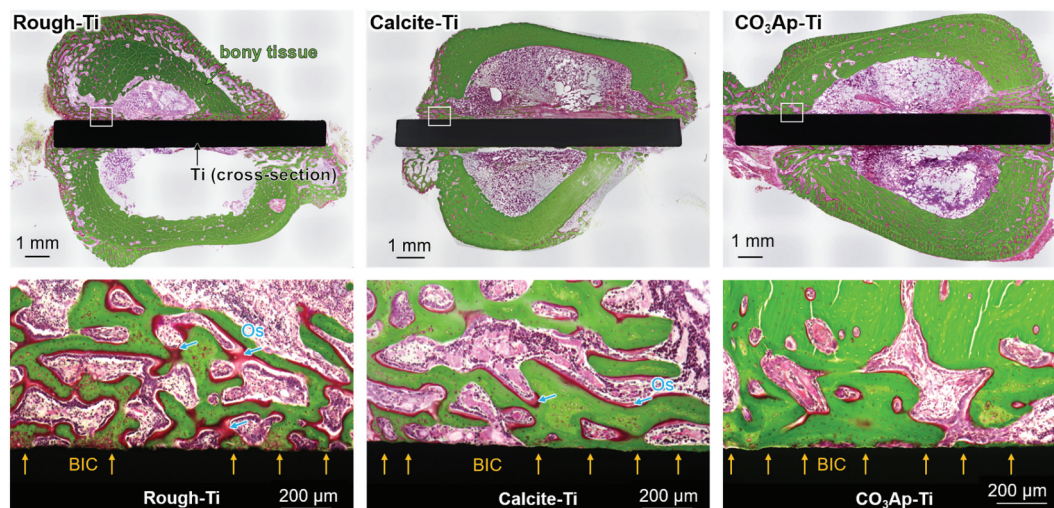
Figure 15. Villanueva-Goldner-stained histological sections: general view, and high-magnification view of the cortical bone of sections in rough-Ti, calcite-Ti, and CO_3Ap-Ti after 4 weeks of healing showing bone-implant contact (BIC) and osteoid (Os). Yellow arrows indicate BIC areas [41].

after implantation in the straight defect of the proximal tibia 2 cm away from the knee joint in rabbits. Abundant mineralized bone formed on the surface of CO_3Ap–Ti. In contrast, osteoid, rather than mineralized bone, was primarily present on the surface of the rough–Ti surface. The bone-implant contact percentages in CO_3Ap–Ti to bone (72.9% ± 6.4%) exceeded those of rough–Ti to bone (48.2 ± 7.8%) and calcite–Ti to bone (59.9 ± 15.4%).

Figure 16 illustrates the detaching test used to measure the adhesion strength of the implant to the bone and the results. The increased bone-implant contact resulted in markedly greater adhesion strengths of CO_3Ap–Ti to bone (42.5 ± 14.7 N) than that of rough-Ti to bone (8.7 ± 4.3 N) and calcite–Ti to bone (24.0 ± 8.9 N). Most of the fracture occurred between at the bone in the case of CO_3Ap–Ti, whereas most of the fracture

occurred at the interface between Ti plate and calcite for calcite–Ti, and interface between Ti plate and bone for rough-Ti. Very high bonding strength with bone and fracture at bone may be caused, at least in part, to the expansion of CO_3Ap in the roughened Ti during the dissolution–precipitation reaction.

The documented excellent tissue response, higher osteoconductivity, and higher adhesion strength guarantee the usefulness of CO_3Ap–Ti for dental and orthopedic implants.

6. Conclusion

Chemically pure (100%) CO_3Ap artificial bone can be fabricated by compositional transformation through
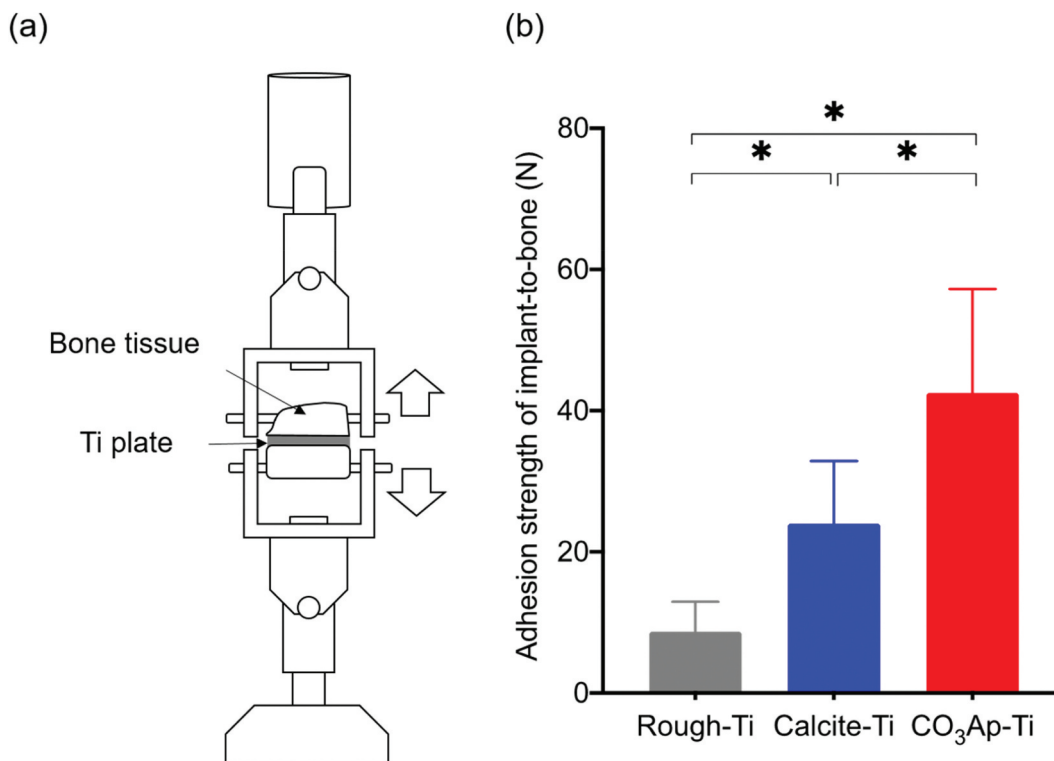
Figure 16. Illustration of the (a) detaching test in bone harvested at 4 weeks after implantation of Ti plates in the tibia defects of rabbits, and (b) adhesion strength of bone-to-implant in rough-Ti, calcite-Ti, and CO_3Ap-Ti (n = 8). *$p < 0.05$ for comparisons between the indicated groups [41].

a dissolution–precipitation reaction using a precursor. Although the results obtained to date are encouraging, little is known about CO_3Ap artificial bone compared with other artificial bones, such as HAp and β-TCP.

Disclosure statement

No potential conflict of interest was reported by the author(s).

References

[1] LeGeros RZ. Calcium phosphates in oral biology and medicine. Basel: Karger; 1991.

[2] Elliot JC. Calcium phosphate biominerals. Rev Miner Geochem. 2002;48:427–453.

[3] Dorozhkin SV, Epple M. Biological and medical significance of calcium phosphates. Angew Chem Int Edit. 2002;41:3130–3146.

[4] Fleet M. Carbonated hydroxyapatite. Singapore: Pan Stanford Publishing Pte; 2015. ISBN: 978-981-4463-67-6.

[5] LeGerous RZ, Ben-Nissan B. Introduction to synthetic and biologic apatites. In: Nissan B, editor. Advances in calcium phosphate biomaterials. Berlin: Springer; 2014. p. 1–17.

[6] Ishikawa K. Bone substitute fabrication based on dissolution-precipitation reaction. Materials. 2010; 3:1138.

[7] Ishikawa K, Matsuya S, Lin X, et al. Fabrication of low crystalline B-type carbonate apatite block from low crystalline calcite block. J Ceram Soc Jpn. 2010;118 (5):341.

[8] Lee Y, Hahm YM, Matsuya S, et al. Characterization of macroporous carbonate-substituted hydroxyapatite bodies prepared in different phosphate solutions. J Mater Sci. 2007;42:7843–7849.

[9] Zaman CT, Takeuchi A, Matsuya S, et al. Fabrication of B-type carbonate apatite blocks by the phosphorylation of free-molding gypsum-calcite composite. Dent Mater J. 2008;27(5):710－－715.

[10] Daitou F, Maruta M, Kawachi G, et al. Fabrication of carbonate apatite block based on internal dissolution-precipitation reaction of dicalcium phosphate and calcium carbonate. Dent Mater J. 2010;29(3):303–308.

[11] Maruta M, Matsuya S, Nakamura S, et al. Fabrication of low-crystalline carbonate apatite foam bone replacement based on phase transformation of calcite foam. Dent Mater J. 2011;30(1):14–20.

[12] Sunouchi K, Tsuru K, Maruta M, et al. Fabrication of solid and hollow carbonate apatite microspheres as bone substitutes using calcite microspheres as a precursor. Dent Mater J. 2012;31(4):549–557.

[13] Ishikawa K, Munar ML, Tsuru K, et al. Fabrication of carbonate apatite honeycomb and its tissue response. J Biomed Mater Res Part A. 2019;107A:1014–1020.

[14] Ishikawa K. Carbonate apatite bone replacement: learn from the bone. J Ceram Soc Jpn. 2019;127 (9):595–601.

[15] Hayashi K, Munar ML, Ishikawa K. Carbonate apatite granules with uniformly sized pores that arrange regularly and penetrate straight through granules in one direction for bone regeneration. Ceram Int. 2019;45 (12):15429–15434.

[16] Fujisawa K, Akita K, Fukuda N, et al. Compositional and histological comparison of carbonate apatite fabricated by dissolution-precipitation reaction and Bio-Oss®. J Mater Sci Mater Med. 2018;29:121.

[17] Hayashi K, Kishida R, Tsuchiya A, et al. Carbonate apatite micro-honeycombed blocks generate bone marrow-like tissues as well as bone. Adv Biosyst. 2019;3:1900140.

[18] Tanaka K, Tsuchiya A, Ogino Y, et al. Fabrication and histological evaluation of a fully interconnected porous CO_3Ap block formed by hydrate expansion of CaO granules. ACS Appl Bio Mater. 2020;3:8872–8878.

[19] Wakae H, Takeuchi A, Udoh K, et al. Fabrication of macroporous carbonate apatite foam by hydrothermal conversion of α-tricalcium phosphate in carbonate solutions. J Biomed Mater Res A. 2018;87(4):957–963.

[20] Takeuchi A, Munar ML, Wakae H, et al. Effect of temperature on crystallinity of carbonate apatite foam prepared from α-tricalcium phosphate by hydrothermal treatment. Biomed Mater Eng. 2019;19(2–3):205–211.

[21] Karashima S, Takeuchi A, Matsuya S, et al. Fabrication of low-crystallinity hydroxyapatite foam based on the setting reaction of alpha-tricalcium phosphate foam. J Biomed Mater Res A. 2009;88 (3):628–633.

[22] Sugiura Y, Tsuru K, Ishikawa K. Fabrication of carbonate apatite foam based on the setting reaction of α-tricalcium phosphate foam granules. Ceram Int. 2016;42:204–210.

[23] Arifta TI, Munar ML, Tsuru K, et al. Fabrication of interconnected porous calcium-deficient hydroxyapatite using the setting reaction of α tricalcium phosphate spherical granules. Cerams Int. 2017;43:11149–11155.

[24] Ishikawa K, Arifta TA, Hayashi K, et al. Fabrication and evaluation of interconnected porous carbonate apatite from alpha tricalcium phosphate spheres. J Biomed Mater Res. 2019;107(2):269–277.

[25] Tsuru K, Kanazawa M, Yoshimoto A, et al. Fabrication of carbonate apatite block through a dissolution–precipitation reaction using calcium hydrogen phosphate dihydrate block as a precursor. Materials. 2017;10(4):374.

[26] Kanazawa M, Tsuru K, Fukuda N, et al. Evaluation of carbonate apatite blocks fabricated from dicalcium phosphate dihydrate blocks for reconstruction of rabbit femoral and tibial defects. J Mater Sci Mater Med. 2017;28(6):85–96.

[27] Lowmunkong R, Sohmura T, Takahashi J, et al. Transformation of 3DP gypsum model to HA by treating in ammonium phosphate solution. J Biomed Mater Res Part B. 2007;80B:386–393.

[28] Lowmunkong R, Sohmura T, Suzuki Y, et al. Fabrication of freeform bone-filling calcium phosphate ceramics by gypsum 3D printing method. J Biomed Mater Res B. 2009;90(2):531–539.

[29] Nomura S, Tsuru K, Matsuya S, et al. Fabrication of carbonate apatite block from set gypsum based on dissolution-precipitation reaction in phosphate-carbonate mixed solution. Dent Mater J. 2014;33(2):166–172.

[30] Ayukawa Y, Suzuki Y, Koyano K, et al. Histological comparison in rats between carbonate apatite fabricated from gypsum and sintered hydroxyapatite on bone remodeling. BioMed Res Int. 2015;2015:Article ID 579541.

[31] Nagai H, Fujioka-Kobayashi M, Fujisawa K, et al. Effects of low crystalline carbonate apatite on proliferation and osteoblastic differentiation of human bone marrow cells. J Mater Sci Mater Med. 2015;26(2):99–107.

[32] Mano T, Akita K, Fukuda N, et al. Histological comparison of three apatitic bone substitutes with different carbonate contents in alveolar bone defects in a beagle mandible with simultaneous implant installation. J Biomed Mater Res. 2020;108(4):1450–1459.

[33] Kudoh K, Fukuda N, Kasugai S, et al. Maxillary sinus floor augmentation using low-crystalline carbonate apatite granules with simultaneous implant installation: first-in-human clinical trial. J Oral Maxil Surg. 2019;77(5):985.e1–985.e11.

[34] Nakagawa T, Fukuda N, Kasugai S, et al. Application of low crystalline carbonate apatite granules in two-stage sinus floor augmentation: a prospective clinical trial and histomorphometric evaluation. J Periodont Imp Sci. 2019;49(6):382–396.

[35] Hayashi K, Kishida R, Tsuchiya A, et al. Honeycomb blocks composed of carbonate apatite, β-tricalcium phosphate, and hydroxyapatite for bone regeneration: effects of composition on biological responses. Mater Today Bio. 2019;4:100031.

[36] Babbush CA, Kent JN, Misiek JD. Titanium Plasma-sprayed (TPS) Screw Implants for the reconstruction of the edentulous mandible. J Oral Maxillofac Surg. 1986;44:274.

[37] Cochran DL, Buser D, ten Bruggenkate CM, et al. The use of reduced healing times on ITI® implants with a sandblasted and acid-etched (SLA) surface: early results from clinical trials on ITI® SLA implants. Clin Oral Implants Res. 2002;13:144.

[38] Albrektsson T, Branemark PI, Hansson HA, et al. Osseointegrated titanium implants. Requirements for ensuring a long-lasting, direct bone-to-implant anchorage in man. Acta Orthop Scand. 1981;52:155.

[39] Shi R, Sugiura Y, Tsuru K, et al. Fabrication of calcite-coated rough-surface titanium using calcium nitrate. Surf Coat Tech. 2018;356:72–79.

[40] Thi BL, Shi R, Long BD, et al. Biological responses of MC3T3-E1 on calcium carbonate coatings fabricated by hydrothermal reaction on titanium. Biomed Mater. 2020;15:035004.

[41] Shi R, Hayashi K, Ishikawa K. Rapid osseointegration bestowed by carbonate apatite coating of rough titanium. Adv Mater Interfaces. 2020;7:2000636.